Macromolecules

pubs.acs.org/Macromolecules Article

Theory and Simulations of Hybrid Networks

Michael Jacobs, Heyi Liang, and Andrey V. Dobrynin*

Cite This: *Macromolecules* 2021, 54, 7337−7346 Read Online

ACCESS | Metrics & More | Article Recommendations

ABSTRACT: Hybrid networks are made of different types of polymer strands, which could differ by their degrees of polymerization (DPs), chemical structure, or rigidity (Kuhn length). Examples of such networks include biological networks and gels cross-linked by binding proteins and networks of graft polymers cross-linked by their side chains. Here, we report on a theoretical model and coarse-grained molecular dynamics simulations of hybrid networks made of two types of strands. The networks are made by cross-linking precursor chains of type 1 by shorter chains of type 2, which results in a trifunctional network with junction points having two strands of type 1 and one strand of type 2. The developed approach, based on the phantom network model and the nonlinear elasticity of the network strands, self-consistently accounts for entropic elasticity, bond deformation, and the continuous redistribution of stress between different network strands as they undergo nonlinear deformation. Analysis of the different deformation regimes shows that at small deformations the network elastic response is controlled by the elasticity of the longest network strands. However, in the nonlinear network deformation regime, the network mechanical properties are determined by nonlinear deformation of the strands of the first kind constituting the majority of the network strands. The model predictions are in excellent agreement with molecular dynamics simulations of hybrid networks in the linear and nonlinear deformation regimes. Furthermore, the model provides a theoretical foundation for the analysis of strain stiffening observed in networks of graft polymers and networks with a bimodal distribution of strands.

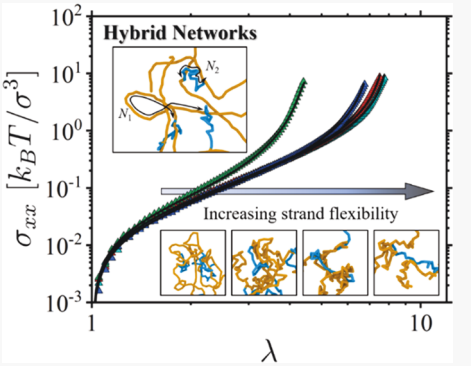

INTRODUCTION

Hybrid networks—networks consisting of different types of strands—play an important role in biophysics and polymer and materials science.[1−13] The strands of such networks could differ by their degrees of polymerization (DPs), chemical structure, and rigidity (Kuhn length), as illustrated in Figure 1. In this respect due to the random, uncontrolled, nature of the cross-linking process, a typical elastomeric network consists of chains with a broad distribution of strand DPs and therefore can be viewed as a hybrid network.[14−16] The mechanical properties of polymeric networks depend on the width of their strand distributions with the shortest ones believed to be the driving force behind network rupture. The majority of biological networks and gels are made by cross-linking biopolymers with various binding proteins that themselves can be highly compliant macromolecules (Figure 1b).[17−19] These networks are examples of hybrid networks made of strands with different chemical structures, DP, and rigidities. The difference in bending rigidities of the network strands dramatically influences the mechanical properties of biological networks and gels in the linear and nonlinear deformation regimes. In particular, these materials can have a linear modulus as low as 1 Pa and can stiffen by a factor of up to 1000 under applied external stress.[18]

Another example of a hybrid network is a network made by cross-linking graft polymers through their side chains (Figure 1c).[20−23] This way of cross-linking produces synthetic networks with brush-like and linear strands. The rigidity of the brush-like strands can be controlled by changing the grafting density of the side chains and their degree of polymerization, while the compliance of the linear chains bridging graft polymers together can be adjusted through variation of the DP of the side chains as well. These networks demonstrate mechanical properties similar to those of biological tissues in solvent-free elastomeric materials and can be viewed as solvent-free synthetic mimics of biological networks and gels.[22,23]

In this paper, we develop a model of hybrid networks made of strands with different DPs and Kuhn lengths to address the networks' mechanical properties in the linear and nonlinear deformation regimes. Our approach fuses the phantom network model,[24−28] which accounts for cross-link fluctuations

Received: April 9, 2021
Revised: June 21, 2021
Published: August 6, 2021

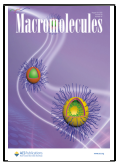

https://doi.org/10.1021/acs.macromol.1c00774
Macromolecules 2021, 54, 7337−7346

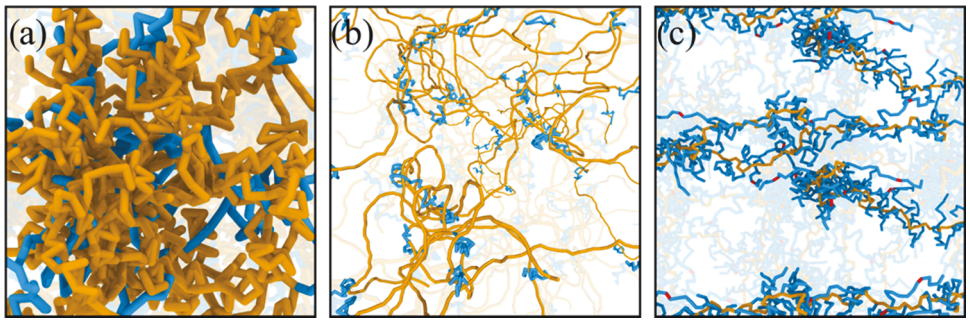

Figure 1. Examples of hybrid networks. Networks made of two types of linear chains (a), networks of semiflexible biological filaments (b), and bottlebrush networks (c).

and a nonlinear expression for the effective chain spring constant, incorporating finite chain extensibility, bending rigidity, and bond stretching.[29] The model predictions are tested against the computer simulation results of hybrid network deformation in the linear and nonlinear deformation regimes. The model is applied to the analysis of deformation data of bimodal networks[30,31] and networks of graft polymers with different molecular architectures.[20−23]

MODEL OF HYBRID NETWORKS

Phantom Network Model. Consider a hybrid network made of two types of strands (see Figure 1a) in which chains of type 1 are connected by chains of type 2, making each connection a trifunctional cross-link. The polymeric strands between cross-links are modeled by elastic springs with the bare strand spring constants k_1 and k_2. For flexible linear chains of type i with DP = N_i, monomer projection length l_i^0, and Kuhn length b_i^0, the chain spring constant is equal to

$$k_i = 3k_BT/N_i l_i^0 b_i^0 \quad (1)$$

where k_B is the Boltzmann constant and T is the absolute temperature.

To describe the elastic properties of hybrid networks, we modify the classical "phantom network model" introduced by James and Guth[24,25] (see for review[26−28]). In the framework of this model, the macroscopic deformation is transmitted to the bulk of the network through the network strands connected to its surface, such that each network strand (chain) is effectively connected to the boundary by a cascading hierarchical set of chains starting from both ends of a strand, as shown in Figure 2. This cascading set of strands defines fluctuations of the network junction points (cross-links) and can be represented by two effective springs connecting a network strand to the affinely deformed elastic background. This reflects a dual role of network strands as they (i) deform themselves upon applied deformation and (ii) contribute to fluctuations of the other chains' junction points. In this respect, the phantom network model is an effective elastic medium model, which self-consistently determines the deformation of individual network strands with fluctuating junction points, substituting them by effective springs. The phantom network model was generalized to incorporate the effects of strand polydispersity,[16] entanglements,[28] and loops[32−34] in network elasticity.

In our formulation of the phantom network model (see Figure 3a), each network strand is substituted by a spring with spring constant k_i (see eq 1). These springs are connected to the affinely deformed elastic background by four effective springs with spring constants k_i^∞ where index i = 1 and 2, as illustrated in Figure 3a for strands of type 2. The strength of the effective spring k_i^∞ is obtained from the recurrence

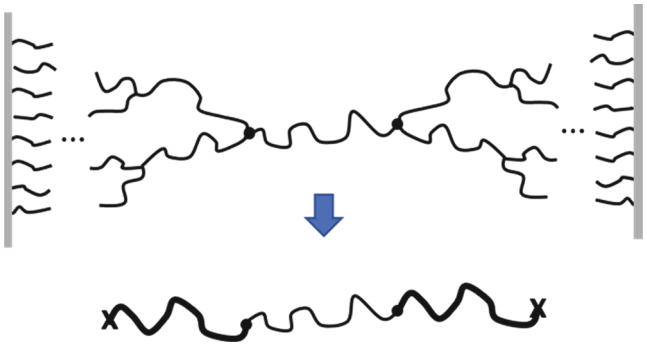

Figure 2. Schematic representation of chains used in calculations of the effective springs in the phantom network model in homopolymer networks.

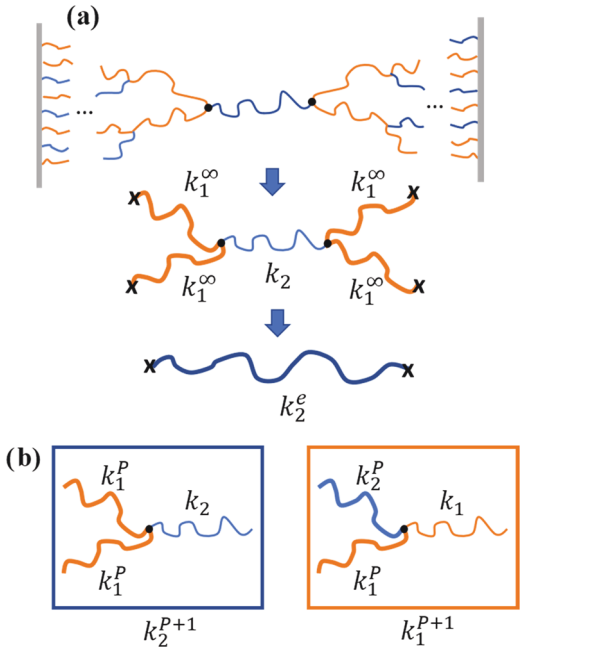

Figure 3. (a) Schematic representation of chains used in calculations of the effective springs of hybrid networks in the phantom network model. The reduction procedure is illustrated for chains of type 2. (b) Diagrammatic representation of the recurrence relations for calculations of the renormalized spring constants.

https://doi.org/10.1021/acs.macromol.1c00774
Macromolecules 2021, 54, 7337−7346

relations between the spring constants of binary tree generation P and those of generation $P + 1$, as illustrated in Figure 3b. For large P ($P \to \infty$) such that $k_i^P \approx k_i^{P+1} \approx k_i^\infty$, the recurrence relations transform into

$$(k_1^\infty)^{-1} = k_1^{-1} + (k_1^\infty + k_2^\infty)^{-1} \tag{2a}$$

$$(k_2^\infty)^{-1} = k_2^{-1} + (2k_1^\infty)^{-1} \tag{2b}$$

After some algebra, the solutions of eqs 2a and 2b are written in the following form

$$k_1^\infty = k_1 \frac{-3 + \sqrt{9 + 16\nu}}{4\nu} \tag{3a}$$

$$k_2^\infty = k_2 \frac{2\nu r}{1 + 2\nu r} \tag{3b}$$

where normalized spring constants $\nu = k_1/k_2$ and $r = k_1^\infty/k_1$ are introduced.

Taking into account network topology (see Figure 3) and the explicit expressions for k_i^∞, we write down equations determining the effective spring constants representing each network strand and connected to the affinely deformed elastic background

$$(k_1^e)^{-1} = k_1^{-1} + 2(k_1^\infty + k_2^\infty)^{-1} \tag{4a}$$

$$(k_2^e)^{-1} = k_2^{-1} + (k_1^\infty)^{-1} \tag{4b}$$

Substituting the explicit expressions for the spring constants k_i^∞ into eqs 4a and 4b, we arrive at the relationships between the effective spring constants and the bare spring constants of network strands k_i and their ratio ν

$$\frac{k_1^e}{k_1} = \phi_1(\nu) = \frac{2}{\sqrt{9 + 16\nu} + 1} \tag{5a}$$

$$\frac{k_2^e}{k_2} = \phi_2(\nu) = \frac{\sqrt{9 + 16\nu} - 3}{\sqrt{9 + 16\nu} + 1} \tag{5b}$$

Note that the calculations of the effective spring constants of individual network strands presented above are based on a tree-like structure of a network without loops or dangling ends.

The shear modulus of a hybrid network with the number density $\rho_{s,i}$ of strands of type i and their mean-square average end-to-end distance $\langle \overline{R}_{\text{in},i}^2 \rangle$ is a sum of contributions from all effective springs within a unit volume

$$G_0 = \frac{1}{3}\rho_{s,1} k_1^e \langle \overline{R}_{\text{in},1}^2 \rangle + \frac{1}{3}\rho_{s,2} k_2^e \langle \overline{R}_{\text{in},2}^2 \rangle \tag{6}$$

Here and below in the text, we use a bar $\overline{\ldots}$ to indicate the average over a strand's conformations and brackets $\langle \ldots \rangle$ to show the average over all strands of this type in a network.

At small deformations, eq 6 can be simplified using the expression for k_i (eq 1), accounting for the constraint imposed by the network topology on strand density, $\rho_{s,1}/\rho_{s,2} = 2$ and assuming that network strands are flexible chains with $\langle \overline{R}_{\text{in},i}^2 \rangle = N_i l_i^0 b_i^0$. Thus, in the linear network deformation regime, the shear modulus of hybrid networks of flexible chains is expressed as follows

$$G_0 = k_B T \rho_{s,1} \left(\phi_1(\nu) + \frac{1}{2}\phi_2(\nu) \right) = k_B T \frac{\rho}{2N_1 + N_2} \tag{7}$$

where the number density of the network strands $\rho_{s,1}$ is obtained from the number density of repeat units

$$\rho = \rho_{s,1} N_1 + \rho_{s,2} N_2 = \rho_{s,1}(N_1 + N_2/2) \tag{8}$$

In a hybrid network of long chains connected by short chains, $N_1 \gg N_2$, eq 7 indicates that such networks behave as networks of long linear chains cross-linked by tetrafunctional cross-links. However, if the opposite inequality holds, $N_1 \ll N_2$, the network shear modulus is proportional to the concentration of the cross-linking chains, ρ/N_2. Thus, in the linear network deformation regimes in both cases, the shear modulus of hybrid networks at small deformations is controlled by the longest chains.

It is also important to point out that the number of repeat units belonging to network strands with DPs N_1 and N_2 are not independent but interrelated through the number fraction of repeat units belonging to strands of type 1, $\varphi = \rho_{s,1} N_1/\rho$, as

$$N_1/N_2 = \varphi/2(1 - \varphi) \tag{9}$$

This relationship allows one to express the shear modulus in terms of the DP of strands of type 1 and network composition φ

$$G_0 = k_B T \frac{\varphi\rho}{2N_1} \tag{10}$$

Thus, one can view the chains of the second kind as an effective solvent diluting the stress supporting strands of the first kind.

Nonlinear Network Deformation. To extend the approach developed above to the nonlinear network deformation regime, we consider deformations of network strands associated with conformational, bending, and bond stretching degrees of freedom. The configurational part of the free energy of the sth network strand of type i can be written as follows[35]

$$F_{\text{conf}}(R_{i,s}, \lambda_{l,i}) = k_B T \frac{R_{\max,i}}{b_i^0} \left(\frac{R_{i,s}^2}{2\lambda_{l,i}^2 R_{\max,i}^2} + \left(1 - \frac{R_{i,s}^2}{\lambda_{l,i}^2 R_{\max,i}^2} \right)^{-1} \right) \tag{11}$$

and is characterized by the end-to-end distance $R_{i,s}$, the number of bonds N_i, bond projection length l_i^0, and Kuhn length b_i^0, which is determined by the chain's bending rigidity K_i (see eq 12 below). In eq 11, we describe the bond and Kuhn length deformation by the bond deformation ratio $\lambda_{l,i} = l_i/l_i^0$ measuring bond extension with respect to its undeformed length l_i^0 and introduce the length of the fully stretched chain with undeformed bonds, $R_{\max,i} = l_i^0 N_i$. For a polymer chain with bending rigidity K_i, its Kuhn length b_i is[36,37]

$$b_i = l_i \frac{1 + \coth K_i - K_i^{-1}}{1 - \coth K_i + K_i^{-1}} \tag{12}$$

At small bond deformations, the bond stretching potential is approximated by a harmonic function with the bond spring constant $K_{b,i}$[35]

$$U_{\text{bond}}(\lambda_{l,i}) = 0.5 K_{b,i} (l_i^0)^2 (\lambda_{l,i} - 1)^2 \tag{13}$$

Combining the configurational and bond stretching contributions to the total free energy of a chain of type i, we have

$$F(R_{i,s}, \lambda_{l,i}) = F_{\text{conf}}(R_{i,s}, \lambda_{l,i}) + N_i U_{\text{bond}}(\lambda_{l,i}) \tag{14}$$

https://doi.org/10.1021/acs.macromol.1c00774
Macromolecules 2021, 54, 7337−7346

The force $\mathbf{f}_{i,s}$ acting on the sth chain of type i (see Figure 4) required to maintain an end-to-end distance $R_{i,s}$ is obtained by

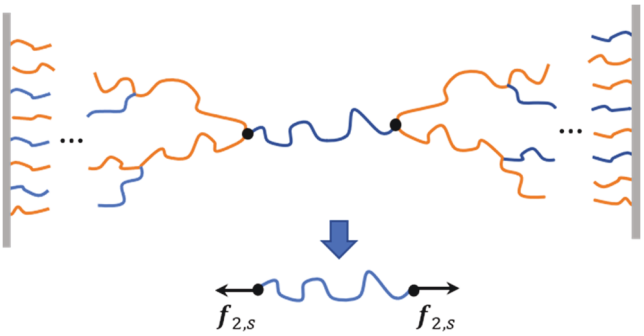

Figure 4. Schematic representation of the reduction of a set of deformed chains connecting a test chain to the boundary by a pair of forces acting on both ends of a chain and maintaining an end-to-end distance.

differentiating the free energy eq 14 with respect to the components of the vector $\mathbf{R}_{i,s}$

$$\mathbf{f}_{i,s} = \mathbf{R}_{i,s}\frac{k_BT}{\lambda_{l,i}^2 R_{\max,i} b_i^0} g(\lambda_{l,i}^{-2} R_{i,s}^2/R_{\max,i}^2) \tag{15}$$

where the function

$$g(x) = (1 + 2(1 - x)^{-2}) \tag{16}$$

We define a spring constant describing the elasticity of strands of type i in the nonlinear deformation regime as the proportionality coefficient between the force and the strand end-to-end vector $\mathbf{R}_{i,s}$ averaged over all strands of this type in a system[35−37]

$$k_i = \frac{k_BT}{\lambda_{l,i}^2 R_{\max,i} b_i^0} g(\lambda_{l,i}^{-2}\langle R_i^2\rangle/R_{\max,i}^2) \tag{17}$$

In writing eq 17, we substituted $\langle g(x)\rangle \approx g(\langle x\rangle)$ and introduced the mean-square average end-to-end distance of network strands of the ith type $\langle R_i^2\rangle$.

The equilibrium bond deformation ratio $\lambda_{l,i}$ for a given value of $R_{i,s}$ is obtained from the minimization of the free energy of the individual network strand (eq 14) with respect to $\lambda_{l,i}$, which after averaging over all network strands of this type in a system reduces to

$$\langle(\mathbf{f}_{i,s}\cdot\mathbf{R}_{i,s})\rangle = N_i K_{b,i}(l_i^0)^2\lambda_{l,i}(\lambda_{l,i} - 1) \approx k_i\langle R_i^2\rangle \tag{18}$$

Note that the last relationship in eq 18 with the approximate sign should only be used to eliminate the divergence of the strand spring constant k_i at strand deformations $\langle R_i^2\rangle \approx R_{\max,i}^2$. The correct analysis of the bond deformation regime requires consideration of the force balance at network vertices, as discussed below.

Equations 15−18 describe the deformation of the network stands in the nonlinear network deformation regime in terms of $\langle R_i^2\rangle$. Now we need to find a relationship between $\langle R_i^2\rangle$ and the first deformation invariant, $I_1 = \lambda_x^2 + \lambda_y^2 + \lambda_z^2$, describing changes in the network dimensions along the x-, y-, and z-directions that are characterized by the corresponding deformation ratios λ_i. In the framework of the phantom network model, each network strand with spring constant k_i is connected to a nonfluctuating background by two springs with spring constants $\tilde{k}_i$. The values of these spring constants are found from the condition that the effective spring constant k_i^e given by eq 4 represents the three springs connected in series, with spring k_i sandwiched between the two springs $\tilde{k}_i$. This representation follows from the middle panel in Figure 3a, if one reduces the assemblies of the two springs at each end of the spring k_i into one effective spring with a spring constant $\tilde{k}_i = k_1^\infty + k_{3-i}^\infty$. Taking this spring arrangement into account and using eq 8, we have

$$(k_i^e)^{-1} = (k_i)^{-1} + 2(\tilde{k}_i)^{-1} \rightarrow \tilde{k}_i = 2k_i\frac{\phi_i(v)}{1 - \phi_i(v)} \tag{19}$$

The mean-square average end-to-end distance $\langle R_i^2\rangle$ of the middle spring for the three-spring assembly is[28,37]

$$\langle R_i^2\rangle = \langle \bar{R}_i^2\rangle + 3\frac{2k_BT}{2k_i + \tilde{k}_i} \tag{20}$$

where in writing down the expression for $\langle \bar{R}_i^2\rangle$ one first averages over all conformations of the sth network strand and after that performs averaging over all strands of this type in a network. Taking into account the affine portion of the deformation of the average end-to-end distance of the sth strand, $\langle \bar{R}_i^2\rangle = \langle \bar{R}_{\text{in},i}^2\rangle I_1/3$, and substituting $\tilde{k}_i$ from eq 19, we arrive at

$$\langle R_i^2\rangle = \frac{\langle \bar{R}_{\text{in},i}^2\rangle I_1}{3} + \frac{3k_BT}{k_i}(1 - \phi_i(v)) \tag{21}$$

This is a self-consistency condition, which allows for calculations of $\langle R_i^2\rangle$ in terms of the first deformation invariant I_1. Note that the affine strand deformations with $\langle R_i^2\rangle \approx I_1\langle \bar{R}_{\text{in},i}^2\rangle/3$ correspond to the case $k_i \rightarrow \infty$. It is worth pointing out that in the derivation of eq 21 it is assumed that all springs are approximated by Gaussian springs with deformation-dependent spring constants (see eq 17) which imposes significant limitations on the applicability of this expression. At best, it could provide a qualitative description of the network strand fluctuations at large chain deformations. However, this crude approximation appears to provide a reasonable crossover function to account for nonlinear strand deformation.

The network shear modulus in the nonlinear network deformation regime is obtained by substituting the nonlinear spring constants given by eq 17 into eqs 3−6

$$G(\langle R_i^2\rangle) = \frac{1}{3}[\lambda_{l,1}^{-2}G_1\phi_1(v)g(\lambda_{l,1}^{-2}\langle R_1^2\rangle/R_{\max,1}^2) + \lambda_{l,2}^{-2}G_2\phi_2(v)g(\lambda_{l,2}^{-2}\langle R_2^2\rangle/R_{\max,2}^2)] \tag{22}$$

where we introduced the network structural modulus associated with strands of the type i

$$G_i = k_BT\rho_{s,i}\langle \bar{R}_{\text{in},i}^2\rangle/R_{\max,i}b_i^0 = k_BT\rho_{s,i}\beta_i\alpha_i^{-1} \tag{23}$$

The parameter α_i is the ratio of the ith strand's Kuhn length b_i^0 to its undeformed contour length, $\alpha_i = b_i^0/N_i l_i^0$. Parameter $\beta_i = \langle \bar{R}_{\text{in},i}^2\rangle/R_{\max,i}^2$, the extensibility ratio, represents the extension of strands of type i in the as-prepared network state. Note that the parameters α_i and β_i are related through the expression for the mean-square end-to-end distance of a semiflexible chain[27]

$$\beta_i = \alpha_i(1 - \alpha_i(1 - \exp(-2/\alpha_i))/2) \tag{24}$$

in the undeformed state. It follows from eq 24 that if there are many Kuhn segments per strand, $\alpha_i^{-1} \gg 1$, the network strand

https://doi.org/10.1021/acs.macromol.1c00774
Macromolecules 2021, 54, 7337−7346

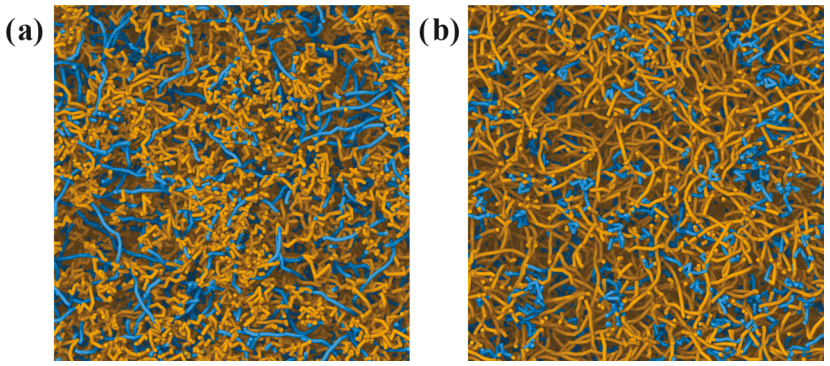

Figure 5. Snapshots of two different types of networks corresponding to the set of network parameters with $\beta_1 < \beta_2$ (a) and $\beta_1 > \beta_2$ (b).

between cross-links behaves as a flexible chain for which $\beta_i \approx \alpha_i \ll 1$. In the opposite limit, $\alpha_i \gg 1$, which corresponds to polymer networks made of rod-like filaments, $\beta_i \approx 1 - 2/3\alpha_i \approx 1$. Furthermore, due to the relationship eq 9, we can express parameters α_2 and β_2 describing properties of the network strands of type 2 in terms of the parameters α_1, β_i and the ratios of the Kuhn lengths b_1^0/b_2^0 and the bond lengths l_1^0/l_2^0.

The expression for the deformation-dependent shear modulus (eq 22) is used to calculate the stress in hybrid networks made of strands with different bending rigidities and DP undergoing uniaxial deformation along the x-axis at a constant volume. For such a system, the deformation ratios are $\lambda_x = \lambda$, $\lambda_y = \lambda_z = 1/\sqrt{\lambda}$ and the first deformation invariant is $I_1 = \lambda^2 + 2/\lambda$. The true stress in a uniaxially deformed network is

$$\sigma_{xx} = (\lambda^2 - \lambda^{-1})G(I_1) \tag{25}$$

Below, we consider two representative cases of hybrid network deformation.

Case $\beta_1 < \beta_2$. This case corresponds to networks in which long flexible strands of the type 1 are cross-linked by short rigid strands of the type 2, as shown in Figure 5a. In this case at small deformations $\langle R_2^2\rangle < R_{\max,2}^2$, the shear modulus is given by eq 22 with $\langle R_i^2\rangle$ obtained from eq 21. As deformation of the network increases and the value of $\langle R_2^2\rangle$ approaches the fully stretched chain limit $R_{\max,2}^2$, the nonlinear spring constant of the strands of the second kind k_2 becomes much larger than k_1 such that the ratio $\nu = k_1/k_2 \ll 1$. In this limit, the corresponding effective spring constants (see eq 8)

$$k_1^{\mathrm{e}} \approx k_1/2 \text{ and } k_2^{\mathrm{e}} \approx 2k_1/3 \tag{26}$$

only depend on the nonlinear spring constant of the strands of the first kind. Taking this into account, the expression for the deformation-dependent shear modulus (eq 22) reduces to

$$G(\langle R_1^2\rangle) \approx \frac{G_1}{6}\left(1 + \frac{2}{3}\frac{\langle \bar{R}_{\mathrm{in},2}^2\rangle}{\langle \bar{R}_{\mathrm{in},1}^2\rangle}\right)\lambda_{l,1}^{-2} g(\lambda_{l,1}^{-2}\langle R_1^2\rangle/R_{\max,1}^2) \tag{27}$$

The prefactor in front of the brackets in eq 27 corresponds to the structural modulus of a tetrafunctional network of strands of type 1. The stress in the network undergoing uniaxial deformation at a constant volume is given by eq 25 with the value of $\langle R_1^2\rangle$ being determined by eq 21 in which the value $\phi_1(\nu) = 1/2$.

To establish what happens with strands of the second kind when upon deformation their size approaches or exceeds $R_{\max,2}$, we have to consider force balance at a network vertex. In each vertex of the network, there are two forces generated by strands of type 1 and one by a strand of type 2. At equilibrium, the sum of these forces is equal to zero such that

$$\mathbf{f}_{1,1} + \mathbf{f}_{1,2} = -\mathbf{f}_{2,3} \tag{28}$$

In eq 28, we use double index notations (i, j) using index i to indicate the type of the strand generating the force and index j to enumerate the strands connected to the vertex. Multiplying both sides of eq 28 by $\mathbf{R}_{2,s}$ and averaging over network vertices, we have

$$2k_1|\langle(\mathbf{R}_1\cdot\mathbf{e}_2)\rangle|N_2 l_2^0\lambda_{l,2} \approx \langle(\mathbf{f}_{2,3}\cdot\mathbf{R}_{2,3})\rangle = N_2 K_{b,2}(l_2^0)^2\lambda_{l,2}(\lambda_{l,2} - 1) \tag{29}$$

where $\mathbf{e}_2$ is a unit vector pointing along the average vector $\mathbf{R}_2$ and we set $\bar{R}_2 \approx N_2 l_2^0\lambda_{l,2}$. It follows from eq 29 that bond deformation will be negligible as long as $2k_1\langle(\mathbf{R}_1\cdot\mathbf{e}_2)\rangle/K_{b,2}l_2^0 \ll 1$, which is controlled by the spring constant k_1 and elongation of the strands of the first kind. Thus, the bond stretching begins when the length of the network strands of the first kind approaches their fully extended chain limit $R_{\max,1}$.

Figure 6 shows network deformation curves calculated using eqs 22 and 27 for the deformation-dependent shear modulus of

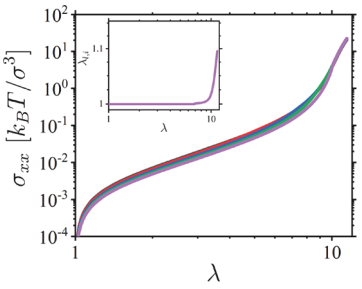

Figure 6. Dependence of network stress on the deformation ratio λ for uniaxially deformed hybrid networks with $N_1 = 200$ and different values of N_2: 20 (black), 50 (red), 100 (blue), 150 (green), and 200 (purple). Network strands are made from identical monomers with bond projection lengths $l_1^0 = l_2^0$, bending constants $K_1 = K_2 = 3$, and bond spring constant $K_{b,i}(l_i^0)^2 = 450\ k_BT$. The inset shows the bond deformation ratio $\lambda_{l,i}$ as a function of λ.

hybrid networks with $l_1^0 = l_2^0$, $K_1 = K_2 = 3$, and $K_{b,1}(l_1^0)^2 = 450\ k_BT$ and degrees of polymerizations $N_1 = 200$ and N_2 varying between 20 and 200. At large λ, all deformation curves converge together.

Case $\beta_1 > \beta_2$. This case represents networks made of short rigid strands of type 1 cross-linked by long flexible strands of type 2 (see Figure 5b). In this case upon deformation, network strands of the first kind approach a fully extended chain limit

https://doi.org/10.1021/acs.macromol.1c00774
Macromolecules 2021, 54, 7337−7346

first. This in turn will result in nonlinear spring constant k_1 (see eq 17) to become much larger than k_2 such that their ratio $\nu = k_1/k_2 \gg 1$. Substituting this relationship into eq 8, we obtain the effective spring constants

$$k_1^e \approx \sqrt{k_1 k_2}/2, \text{ and } k_2^e \approx k_2 \tag{30}$$

and derive the following expression for the network shear modulus at large deformations

$$G(\langle R_i^2 \rangle) \approx \frac{G_1}{6}\sqrt{\frac{R_{\max,1} b_1^0}{R_{\max,2} b_2^0}} \sqrt{\lambda_{l,1}^{-2} g(\lambda_{l,1}^{-2}\langle R_1^2\rangle/R_{\max,1}^2)\lambda_{l,2}^{-2} g(\lambda_{l,2}^{-2}\langle R_2^2\rangle/R_{\max,2}^2)} \tag{31}$$

Note that since the properties of the network are determined by the shortest chains, we can use eq 22 in the entire deformation regime. We derive eq 31 to illustrate what effect softer chains have on the network elasticity and the unexpected geometric mean expression for the effective spring constant in eq 30.

In Figure 7, we plot network stress as a function of the deformation ratio λ calculated using eq 25 with the shear modulus given by eqs 22 and 31. These deformation curves correspond to hybrid networks with $l_1^0 = l_2^0$, $K_1 = K_2 = 3$, and $K_{b,1}(l_1^0)^2 = 450\ k_BT$ and degrees of polymerizations $N_2 = 200$ and N_1 varying between 20 and 200. By changing the degree of polymerization of the strands of the first kind, we increase the value of β_1 shifting the crossover to the nonlinear deformation regime and the associated bond deformation to the left in terms of the deformation ratio λ.

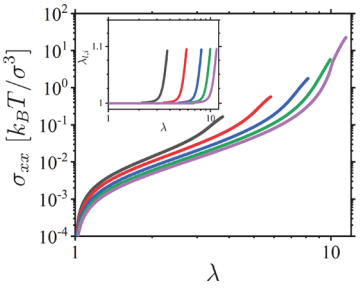

Figure 7. Dependence of the network stress on the deformation ratio λ for uniaxially deformed hybrid networks with $N_2 = 200$ and different values of N_1: 20 (black), 50 (red), 100 (blue), 150 (green), and 200 (purple). Network strands are made from identical monomers with bond projection lengths $l_1^0 = l_2^0$, bending constants $K_1 = K_2 = 3$, and bond spring constant $K_{b,i}(l_i^0)^2 = 450\ k_BT$. The inset shows the bond deformation ratio $\lambda_{l,i}$ as a function of λ.

Thus, the main conclusion of the analysis of the nonlinear network deformation is that in this regime the properties of networks are determined by the extensibility of the strands of the first kind.

SIMULATIONS OF HYBRID NETWORKS

Simulation Details. We tested the predictions of the model of the deformation of hybrid networks in coarse-grained molecular dynamics simulations of the deformation of dense phantom networks of linear chains, as shown in Figure 8. The chains forming the network were modeled by bead-spring chains consisting of monomers with diameter σ. The connectivity of beads in polymer chains and the cross-link bonds were described by the finitely extensible nonlinear elastic (FENE) potential,[38]

$$U_{\text{FENE}}(r) = -0.5 k_s R_{\max,l}^2 \ln(1 - r^2/R_{\max,l}^2) \tag{32}$$

where k_s is the spring constant set to $k_s = 100\ k_BT/\sigma^2$ and the maximum bond length is $R_{\max,l} = 1.5\sigma$. (The large value of the spring constant was selected to minimize the effect of bond stretching at large network deformations). The repulsive part of the bond potential was modeled by the shifted Lennard-Jones potential with the value of the Lennard-Jones interaction parameter $\varepsilon_{LJ} = 1.0\ k_BT$. For this set of parameters, the bond length $l_0 = 0.903\sigma$. The chain bending rigidity was introduced into the model through a bending potential controlling the mutual orientations between two neighboring unit bond vectors $\mathbf{n}_i$ and $\mathbf{n}_{i+1}$ along the polymer backbone

$$U_{i,i+1}^{\text{bend}} = k_BTK(1 - (\mathbf{n}_i \cdot \mathbf{n}_{i+1})) \tag{33}$$

The value of the bending constant K was varied between 0.1 and 10. Thus, for the studied interval of the bending constants K, the corresponding values of the Kuhn length were varied between 0.98σ and 17.5σ. We did not have any additional interactions between monomers.

Networks were prepared by cross-linking a precursor melt of chains with DP = 512 by shorter chains with $N_2 = 20$. The cross-linking algorithm allowed us to obtain a narrow distribution of chains of the first kind with the number average

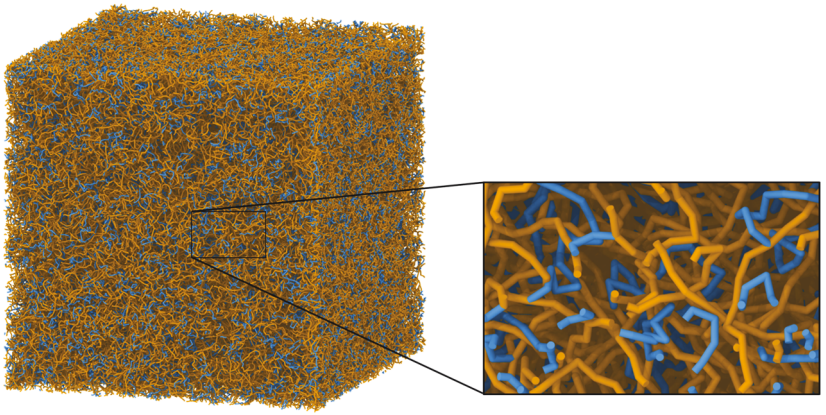

Figure 8. Snapshot of the simulation box.

https://doi.org/10.1021/acs.macromol.1c00774
Macromolecules 2021, 54, 7337−7346

degree of polymerization $\langle N_1 \rangle \approx 32$ by setting every 32nd bead on the backbone chains to be available for cross-linking. The number density of strands of type 1 is equal to $\rho_{s,1} = 0.0310\ \sigma^{-3}$ and of type 2 is $\rho_{s,2} = 0.0165\ \sigma^{-3}$. The fact that $\rho_{s,1} < 2\rho_{s,2}$ is due to the existence of dangling ends of type 1.

Simulations were carried out in a constant number of particles, volume, and temperature ensemble with periodic boundary conditions. The constant temperature was maintained by coupling the system to a Langevin thermostat. The equation of motion of the ith bead is

$$m\frac{d\mathbf{v}_i(t)}{dt} = \mathbf{F}_i(t) - \zeta \mathbf{v}_i(t) + \mathbf{F}_i^R(t) \tag{34}$$

where $\mathbf{v}(t)$ is the ith bead velocity and $\mathbf{F}_i(t)$ is the net deterministic force acting on the ith bead with mass m, which is set to unity in our simulations. $\mathbf{F}_i^R(t)$ is the stochastic force with zero average value $\langle \mathbf{F}_i^R(t) \rangle = 0$ and δ-functional correlations $\langle \mathbf{F}_i^R(t) \cdot \mathbf{F}_i^R(t') \rangle = 6\xi k_B T \delta(t - t')$. The friction coefficient ζ was set to $\zeta = 0.143 m/\tau_{LJ}$, where τ_{LJ} is the standard LJ-time $\tau_{LJ} = \sigma\sqrt{m/\varepsilon}$, where $\varepsilon/k_B T = 1.0$. The velocity-Verlet algorithm with a time step $\Delta t = 0.005\tau_{LJ}$ was used for the integration of the equations of motion (eq 34). All simulations were performed using LAMMPS.[39]

The stress in the uniaxially deformed networks undergoing incremental uniaxial deformation at a constant volume was calculated from the pressure tensor following the standard procedure.[37,40]

Analysis of the Simulation Results. In Figure 9, we test the assumption of the redistribution of stress between short

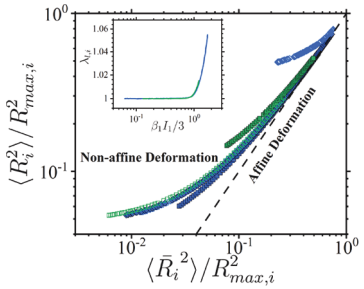

Figure 9. Ratio $\langle R_i^2 \rangle / R^2_{\max,i}$ of the mean-square end-to-end distance $\langle R_i^2 \rangle$ of stress-supporting strands of type i to the square of the end-to-end distance of the fully elongated strand $R^2_{\max,i}$ as a function of the affine part of the strand deformation $\langle \bar{R}_i^2 \rangle / R^2_{\max,i}$ for networks of chains with $\langle N_1 \rangle = 32$, $N_2 = 20$, and different values of K_1 and K_2: $K_1 = 1$ and $K_2 = 0.1$ (blue squares), $K_1 = 1$ and $K_2 = 10$ (blue rhombs), and $K_1 = 3$ and $K_2 = 0.1$ (green squares). Filled symbols denote chains of type 1, and open symbols denote chains of type 2. The dashed line indicates affine deformation, and points above this line are nonaffinely deformed due to the contribution of fluctuations. The inset shows the dependence of the bond deformation ratios $\lambda_{l,1}$ (solid lines) and $\lambda_{l,2}$ (dashed lines) on $\beta_1 I_1/3$, where $\beta_1 = \langle \bar{R}^2_{\text{in},1} \rangle / R^2_{\max,1}$ is the elongation ratio of the longest strands.

and long network strands by plotting the mean-square values of the end-to-end distance $\langle R_i^2 \rangle$ normalized by their corresponding $R^2_{\max,i}$ as a function of $\langle \bar{R}_i^2 \rangle / R^2_{\max,i}$ in the deformed networks. It follows from this figure that both types of strands approach their fully extended chain limit and begin to deform affinely when strands of type 1 demonstrate strong nonlinear deformation. Furthermore, in this deformation regime, both data sets corresponding to strands of type 1 (filled symbols) and type 2 (open symbols) begin to converge indicating a crossover to the affine deformation regime of almost fully extended network strands, in which elastic response is dominated by individual bond elongation and is independent of the initial chain bending constant.

Figure 10 shows stress-deformation curves of a series of hybrid networks. By changing the Kuhn length of the "cross-

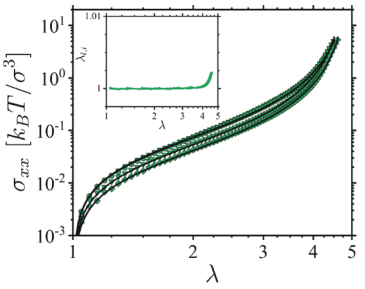

Figure 10. Dependence of the network stress on the elongation ratio λ for hybrid networks of chains with identical bond lengths, $\langle N_1 \rangle = 32$, $K_1 = 3$, $N_2 = 20$, and different values of K_2: 0.1 (squares), 0.3 (circles), 3 (inverted triangles), and 10 (rhombs). Solid lines are best fits to eq 25 with $G(I_1)$ given by eq 22 with fitting parameters (G_1, G_2, β_1, β_2) equal to (29, 34, 0.13, 0.10) for $K_2 = 0.1$, (29, 32, 0.13, 0.11) for $K_2 = 0.3$, (29, 7.9, 0.13, 0.13) for $K_2 = 3$, and (29, 2.7, 0.12, 0.13) for $K_2 = 10$, where G_1 and G_2 have units of $10^{-3}\ k_B T/\sigma^3$. The inset shows dependence of the bond deformation ratios $\lambda_{l,1}$ (solid lines) and $\lambda_{l,2}$ (dashed lines) on λ.

linking" chains, we cover both cases of the network deformation discussed in the previous section. Convergence of the deformation curves at large network deformation clearly indicates that in the nonlinear deformation regime network properties are controlled by deformation of the network strands of the first kind. Note that the bonds begin to deform when type 1 chains approach their fully extended chain limit.

At small deformations, however, both types of chains contribute to the network shear modulus. In particular, with increasing rigidity of the cross-linking chains (increasing their Kuhn length), networks become softer. The solid lines in Figure 10 correspond to network stress calculated using eq 25. For flexible chains with $K_2 < 1$, we use more the general form of the function[35,37]

$$g(x_i) = \left(3 + 2\frac{b_i^0}{l_i^0}\left[\sqrt{K_i^2 + (1 - x_i)^{-2}} - \sqrt{K_i^2 + 1}\right]\right) \tag{35}$$

The good agreement between the analytical calculations and simulation results validates the approximations that have been used for the evaluation of the nonlinear spring constants.

The data shown in Figure 11 further corroborate our model predictions that network strands of type 1 determine the network nonlinear response. For this figure, we keep the properties of the cross-linking chains of type 2 constant and changed the bending rigidity constant K_1 of the strands of the first kind between 0.1 and 3. By increasing K_1 values, we increase the chain elongation ratio β_1 moving the crossover to the nonlinear network deformation regime to smaller λ values since at the crossover $\lambda \approx 1/\sqrt{\beta_1}$. This crossover correlates with the onset of bond deformation as evident from the inset.

COMPARISON WITH EXPERIMENTS

Our model provides the theoretical foundation for analysis of the strain stiffening in networks of graft polymers (combs and

https://doi.org/10.1021/acs.macromol.1c00774
Macromolecules 2021, 54, 7337−7346

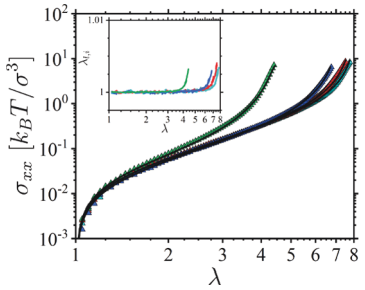

Figure 11. Dependence of the network stress on the elongation ratio λ for hybrid networks of chains with identical bond lengths $K_2 = 1$, $N_2 = 20$, $\langle N_1 \rangle = 32$, and different values of K_1: 0.1 (cyan triangles), 0.3 (red triangles), 1 (blue triangles), and 3 (green triangles). Solid lines are best fits to eq 25 with $G(I_1)$ given by eq 22 with fitting parameters (G_1, G_2, β_1, β_2) equal to (41, 7.9, 0.044, 0.049) for $K_1 = 0.1$, (41, 7.6, 0.050, 0.047) for $K_1 = 0.3$, (33, 6.8, 0.064, 0.042) for $K_1 = 1$, and (35, 1.9, 0.155, 0.01) for $K_1 = 3$, where G_1 and G_2 have units of 10^{-3} k_BT/σ^3. The inset shows dependence of the bond deformation ratios $\lambda_{l,1}$ (solid lines) and $\lambda_{l,2}$ (dashed lines) on λ.

bottlebrushes) cross-linked by their side chains.[23] According to our model, the mechanical properties of such networks are determined by the strands of the first kind, which in this case are graft polymers. The validity of this simplification was confirmed in several studies of strain stiffening in networks of comb and bottlebrush macromolecules.[20−23] Figure 12 shows

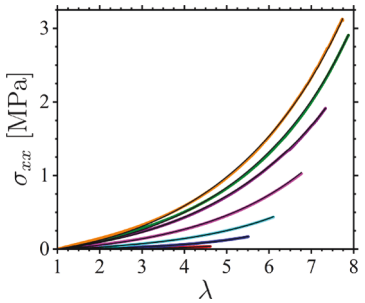

Figure 12. Dependence of the network stress on the elongation ratio λ for bottlebrush polymers cross-linked through their side chains, with the backbone network strand DP $N_1 = 600$, DP of the side chains $n_{sc} = N_2/2 = 14$, and side chains grafted onto every n_gth backbone monomer, where $n_g = 1$ (red), 2 (blue), 4 (cyan), 8 (magenta), 16 (purple), 32 (green), and 64 (orange). Black lines are best fits to eq 36, with fitting parameters (G, β) equal to (0.86 kPa, 0.055) for $n_g = 1$, (3.02 kPa, 0.034) for $n_g = 2$, (7.81 kPa, 0.020) for $n_g = 4$, (15.1 kPa, 0.016) for $n_g = 8$, (25.2 kPa, 0.012) for $n_g = 16$, (28.4 kPa, 0.014) for $n_g = 32$, and (33.7 kPa, 0.013) for $n_g = 64$. Data from ref 23.

the dependence of the stress in networks of bottlebrush polymers cross-linked through their side chains. The experimental data are fitted by the following expression

$$\sigma_{xx} = G(\lambda^2 - \lambda^{-1})g(\beta I_1/3)/3 \quad (36)$$

in which structural modulus G and elongation ratio β are fitting parameters.

We apply the approach developed here to describe the deformation of end-linked polydimethylsiloxane chains made of short chains with $M_n = 1.1 \times 10^3$ g/mol and long chains with $M_n = 18.5 \times 10^3$ g/mol.[30,31] The molar fraction of the shorter chains is varied between 60 and 95%. The longer strands with such molar mass can also entangle; therefore, to account for this effect, we added the Mooney−Rivlin term describing the effect of entanglements in the linear deformation regime[29]

$$\sigma_{xx} = (\lambda^2 - \lambda^{-1})(G_e/\lambda + Gg(\beta I_1/3)/3) \quad (37)$$

where G_e is the shear modulus associated with the entanglements. Figure 13 presents experimental data and

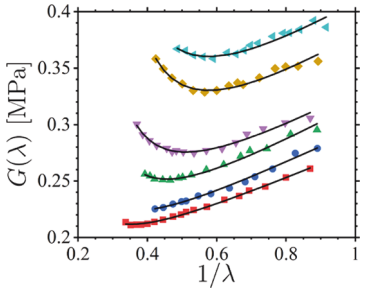

Figure 13. Dependence of the deformation-dependent modulus $G(\lambda) = \sigma_{xx}/(\lambda^2 - \lambda^{-1})$ on the reciprocal elongation ratio $1/\lambda$ for end-linked polydimethylsiloxane chains with bimodal distribution of their molecular weights ($M_n = 1.1 \times 10^3$ g/mol and 18.5×10^3 g/mol), with the molar fraction of the shorter chains equal to 62.8% (red squares), 70.0% (green triangles), 77.0% (blue circles), 83.4% (purple inverted triangles), 89.4% (gold rhombs), and 95.0% (cyan left triangles). Black lines are best fits to eq 37, with fitting parameters (G, G_e, β) equal to (146 kPa, 125 kPa, 0.033) for 62.8%, (142 kPa, 159 kPa, 0.080) for 70.0%, (146 kPa, 139 kPa, 0.042) for 77.0%, (156 kPa, 149 kPa, 0.098) for 83.4%, (176 kPa, 164 kPa, 0.134) for 89.4%, and (205 kPa, 163 kPa, 0.122) for 95.0%. Data from ref 30.

fitting results to eq 37 with the three fitting parameters G, G_e, and β. Indeed, analysis of the experimental data clearly indicates that networks become softer as the fraction of longer chains increases with the longest network strands controlling the crossover to the nonlinear network deformation regime. In particular, the values of the parameter β decrease with the decreasing molar fraction of the short chains, pointing out the increase of the effective degree of polymerization of the longer chains. The structural modulus G changes between 146 and 205 kPa, demonstrating a 40% increase as the molar fraction of short chains changes between 63 and 95%. The entanglement shear modulus shows a much weaker variation with the molar fraction, changing between 125 and 164 kPa and beginning to saturate as the molar fraction exceeds 84%.

CONCLUSIONS

We developed a theoretical model of hybrid networks, made of two different types of strands, covering both the linear and nonlinear deformation regimes. The network shear modulus is obtained in the framework of the phantom network model by calculating the effective spring constants associated with each network strand. To account for nonlinear strand deformation, we describe the strands as nonlinear springs with conformational, bending, and bond stretching degrees of freedom. At small deformations, the model predicts that the network shear modulus is controlled by the longest network strands. However, in the nonlinear deformation regime, the network elastic response is dominated by the strands of the first kind. In particular, in the case of a network made with short strands of the first kind, their effective spring constant is proportional to the geometric mean of the bare spring constants of both types of strands (see eq 31).

https://doi.org/10.1021/acs.macromol.1c00774
Macromolecules 2021, 54, 7337−7346

The model predictions are in a very good agreement with coarse-grained molecular dynamics simulations of hybrid networks. The stress-deformation curves obtained in simulations overlap with theoretical curves, as shown in Figures 10 and 11. Note that the analysis of the individual strand deformations and location of the crossover to the bond deformation regime confirms the assumptions made in the model's development. Furthermore, our model describes the deformation of networks with graft polymer strands and bimodal networks reasonably well, as illustrated in Figures 12 and 13.

We hope that the success of the model in describing the simulation results and deformation of networks of graft polymers and bimodal networks will inspire the application of the model to the analysis of mechanical properties of the hybrid network made of synthetic and/or biological macromolecules.

AUTHOR INFORMATION

Corresponding Author

Andrey V. Dobrynin − *Department of Chemistry, University of North Carolina at Chapel Hill, Chapel Hill, North Carolina 27399, United States;* orcid.org/0000-0002-6484-7409; Email: avd@email.unc.edu

Authors

Michael Jacobs − *Department of Chemistry, University of North Carolina at Chapel Hill, Chapel Hill, North Carolina 27399, United States;* orcid.org/0000-0002-7255-3451

Heyi Liang − *Pritzker School of Molecular Engineering, University of Chicago, Chicago, Illinois 60637, United States;* orcid.org/0000-0002-8308-3547

Complete contact information is available at: https://pubs.acs.org/10.1021/acs.macromol.1c00774

Notes

The authors declare no competing financial interest.

ACKNOWLEDGMENTS

This work was supported by the National Science Foundation under the Grants DMREF- 2049518.

REFERENCES

(1) Boyce, M. C.; Arruda, E. M. Constitutive models of rubber elasticity: A review. *Rubber Chem. Technol.* **2000**, *73*, 504−523.

(2) Bausch, A. R.; Kroy, K. A bottom-up approach to cell mechanics. *Nat. Phys.* **2006**, *2*, 231−238.

(3) Broedersz, C. P.; Kasza, K. E.; Jawerth, L. M.; Munster, S.; Weitz, D. A.; MacKintosh, F. C. Measurement of nonlinear rheology of cross-linked biopolymer gels. *Soft Matter* **2010**, *6*, 4120−4127.

(4) Broedersz, C. P.; Sheinman, M.; MacKintosh, F. C. Filament-Length-Controlled Elasticity in 3D Fiber Networks. *Phys. Rev. Lett.* **2012**, *108*, No. 108078102.

(5) Broedersz, C. P.; Storm, C.; MacKintosh, F. C. Nonlinear elasticity of composite networks of stiff biopolymers with flexible linkers. *Phys. Rev. Lett.* **2008**, *101*, No. 850121801.

(6) Brown, A. E. X.; Litvinov, R. I.; Discher, D. E.; Purohit, P. K.; Weisel, J. W. Multiscale Mechanics of Fibrin Polymer: Gel Stretching with Protein Unfolding and Loss of Water. *Science* **2009**, *325*, 741−744.

(7) Das, M.; MacKintosh, F. C.; Levine, A. J. Effective medium theory of semiflexible filamentous networks. *Phys. Rev. Lett.* **2007**, *99*, No. 99038101.

(8) Discher, D. E.; Janmey, P.; Wang, Y. L. Tissue cells feel and respond to the stiffness of their substrate. *Science* **2005**, *310*, 1139−1143.

(9) Gardel, M. L.; Kasza, K. E.; Brangwynne, C. P.; Liu, J. Y.; Weitz, D. A. Mechanical Response of Cytoskeletal Networks. *Methods Cell Biol.* **2008**, *89*, 487−519.

(10) Gardel, M. L.; Nakamura, F.; Hartwig, J. H.; Crocker, J. C.; Stossel, T. P.; Weitz, D. A. Prestressed F-actin networks cross-linked by hinged filamins replicate mechanical properties of cells. *Proc. Nat. Acad. Sci. U.S.A.* **2006**, *103*, 1762−1767.

(11) Janmey, P. A.; McCormick, M. E.; Rammensee, S.; Leight, J. L.; Georges, P. C.; Mackintosh, F. C. Negative normal stress in semiflexible biopolymer gels. *Nat. Mater.* **2007**, *6*, 48−51.

(12) Storm, C.; Pastore, J. J.; MacKintosh, F. C.; Lubensky, T. C.; Janmey, P. A. Nonlinear elasticity in biological gels. *Nature* **2005**, *435*, 191−194.

(13) Trepat, X.; Deng, L. H.; An, S. S.; Navajas, D.; Tschumperlin, D. J.; Gerthoffer, W. T.; Butler, J. P.; Fredberg, J. J. Universal physical responses to stretch in the living cell. *Nature* **2007**, *447*, 592−595.

(14) Mark, J. E. Some recent theory, experiments, and simulations on rubberlike elasticity. *J. Phys. Chem. B* **2003**, *107*, 903−913.

(15) Treloar, L. R. G. *The Physics of Rubber Elasticity*; Clarendon Press: Oxford, 2005.

(16) Higgs, P. G.; Ball, R. C. Polydisperse polymer networks: elasticity, orientational properties, and small angle neutron scattering. *J. Phys.* **1988**, *49*, 1785−1811.

(17) Kasza, K. E.; Broedersz, C. P.; Koenderink, G. H.; Lin, Y. C.; Messner, W.; Millman, E. A.; Nakamura, F.; Stossel, T. P.; MacKintosh, F. C.; Weitz, D. A. Actin Filament Length Tunes Elasticity of Flexibly Cross-Linked Actin Networks. *Biophys. J.* **2010**, *99*, 1091−1100.

(18) Kroy, K. Elasticity, dynamics and relaxation in biopolymer networks. *Curr. Opin. Colloid Interface Sci.* **2006**, *11*, 56−64.

(19) Lee, H.; Pelz, B.; Ferrer, J. M.; Kim, T.; Lang, M. J.; Kamm, R. D. Cytoskeletal Deformation at High Strains and the Role of Cross-link Unfolding or Unbinding. *Cell. Mol. Bioeng.* **2009**, *2*, 28−38.

(20) Liang, H.; Sheiko, S. S.; Dobrynin, A. V. Supersoft and Hyperelastic Polymer Networks with Brushlike Strands. *Macromolecules* **2018**, *51*, 638−645.

(21) Liang, H.; Vatankhah-Varnoosfaderani, M.; Sheiko, S. S.; Dobrynin, A. V. Computationally Driven Design of Soft Materials with Tissue-like Mechanical Properties. In *Gels and Other Soft Amorphous Solids*; Horkay, F.; Douglas, J. F.; Del Gado, E., Eds.; American Chemical Society: Washington, DC, 2019; pp 33−50.

(22) Vatankhah-Varnoosfaderani, M.; Daniel, W. F.; Zhushma, A. P.; Li, Q.; Morgan, B. J.; Matyjaszewski, K.; Armstrong, D. P.; Spontak, R. J.; Dobrynin, A. V.; Sheiko, S. S. Bottlebrush Elastomers: A New Platform for Freestanding Electroactuation. *Adv. Mater.* **2017**, *29*, No. 1604209.

(23) Vatankhah-Varnosfaderani, M.; Daniel, W. F. M.; Everhart, M. H.; Pandya, A. A.; Liang, H.; Matyjaszewski, K.; Dobrynin, A. V.; Sheiko, S. S. Mimicking Biological Stress-Strain Behavior with Synthetic Elastomers. *Nature* **2017**, *549*, 497−501.

(24) James, H. M.; Guth, E. Theory of the increase in rigidity of rubber during cure. *J. Chem. Phys.* **1947**, *15*, 669−683.

(25) James, H. M. Statistical properties of networks of flexible chains. *J. Chem. Phys.* **1947**, *15*, 651−668.

(26) Flory, P. J. Statistical thermodynamics of random networks. *Proc. R. Soc. London, Ser. A* **1976**, *351*, 351−380.

(27) Rubinstein, M.; Colby, R. H. *Polymer Physics*; Oxford University Press: New York, 2003.

(28) Rubinstein, M.; Panyukov, S. Elasticity of polymer networks. *Macromolecules* **2002**, *35*, 6670−6686.

(29) Dobrynin, A. V.; Carrillo, J.-M. Y. Universality in nonlinear elasticity of biological and polymeric networks and gels. *Macromolecules* **2011**, *44*, 140−146.

(30) Andrady, A. L.; Llorente, M. A.; Mark, J. E. Model networks of end-linked polydimethylsiloxane chains. VII. Networks designed to

demonstrate non-Gaussian effects related to limited chain extensibility. *J. Chem. Phys.* **1980**, *72*, 2282−2290.
(31) Andrady, A. L.; Llorente, M. A.; Mark, J. E. Model networks of end-linked polydimethylsiloxane chains. IX Gaussian, non-Gaussian, and ultimate properties of the trifunctional networks. *J. Chem. Phys.* **1980**, *73*, 1439−1445.
(32) Zhong, M.; Wang, R.; Kawamoto, K.; Olsen, B. D.; Johnson, J. A. Quantifying the impact of molecular defects on polymer network elasticity. *Science* **2016**, *353*, 1264−1268.
(33) Lin, T.-S.; Wang, R.; Johnson, J. A.; Olsen, B. D. Revisiting the elasticity theory for real Gaussian phantom networks. *Macromolecules* **2019**, 1685−1694.
(34) Lang, M. J. Elasticity of phantom model networks with cyclic defects. *ACS Macro Lett.* **2018**, 536−539.
(35) Jacobs, M.; Dobrynin, A. V. Deformation model of chains and networks with extendable bonds. *Macromolecules* **2020**, *53*, 10874−10881.
(36) Dobrynin, A. V.; Carrillo, J.-M. Y.; Rubinstein, M. Chains are more flexible under tension. *Macromolecules* **2010**, *43*, 9181−9190.
(37) Carrillo, J.-M. Y.; Mackintosh, F. C.; Dobrynin, A. V. Nonlinear elasticity: From single chain to networks and gels. *Macromolecules* **2013**, *46*, 3679−3692.
(38) Kremer, K.; Grest, G. S. Dynamics of entangled linear polymer melts: A molecular dynamics study. *J. Chem. Phys.* **1990**, *92*, 5057−5086.
(39) Plimpton, S. J. Fast parallel algorithms for short-range molecular dynamics. *J. Comput. Phys.* **1995**, *117*, 1−19. lammps.sandia.gov
(40) Grest, G. S.; Putz, M.; Everaers, R.; Kremer, K. Stress-strain relation of entangled polymer networks. *J. Non-Cryst. Solids* **2000**, *274*, 139−146.

https://doi.org/10.1021/acs.macromol.1c00774
Macromolecules 2021, 54, 7337−7346